ACS APPLIED MATERIALS & INTERFACES

Research Article

www.acsami.org

# Detection of Protein Conformational Changes with Multilayer Graphene Nanopore Sensors

Wanzhi Qiu[†,‡] and Efstratios Skafidas*[,†,‡]

[†]Centre for Neural Engineering, The University of Melbourne, 203 Bouverie Street, Carlton, Victoria 3053, Australia

[‡]Department of Electrical and Electronic Engineering, The University of Melbourne, Parkville, Victoria 3010, Australia

Supporting Information

**ABSTRACT:** Detecting conformational change in protein or peptide is imperative in understanding their dynamic function and diagnosing diseases. Existing techniques either rely on ensemble average that lacks the necessary sensitivity or require florescence labeling. Here we propose to discriminate between different protein conformations with multiple layers of graphene nanopore sensors by measuring the effect of protein-produced electrostatic potential (EP) on electric transport. Using conformations of the octapeptide Angiotensin II obtained through molecular dynamics simulations, we show that the EP critically depends on the geometries of constituent atoms and each conformation carries a unique EP signature. We then, using quantum transport simulations, reveal that these characteristic EP profiles cause distinctive modulation to electric charge densities of the graphene nanopores, leading to distinguishable changes in conductivity. Our results open the potential of label-free, single-molecule, and real-time detection of protein conformational changes.

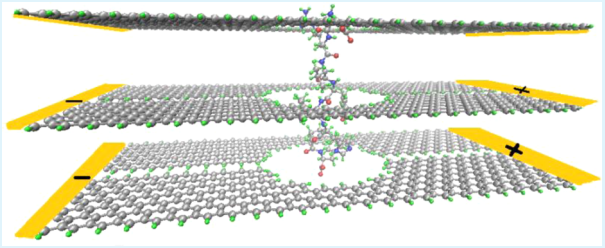

**KEYWORDS:** *protein conformational change, graphene nanopores, biosensors, electrostatic potential, quantum conductance*

## 1. INTRODUCTION

Proteins are biological molecules consisting of chains of amino acids. They are fundamental components of all living cells; performing a variety of biological tasks such as intercellular signaling, defending against foreign substances, catalyzing chemical and biological reactions, and regulating metabolism. Protein polymers with shorter amino acids chains are often called peptides. Sharing similar structural and functional properties, both proteins and peptides have received enormous attention in molecular biology.[1]

The biological functions of proteins depend on their ability to recognize and bind to other molecules. For example, antibody proteins bind to particular foreign substances that fit their binding sites. Enzymes recognize and bind to specific substrates in order to facilitate chemical reactions. Messenger proteins pass signals from one cell to another by binding to receptor sites on proteins in the membrane of the receiving cell. In order to perform various tasks proteins transit into different conformations which are twisted, folded, and coiled into particular shapes. As a result, protein or peptide folding has become an increasingly important field in current molecular biology.[2] Much effort has been devoted to understanding the conformational structures of proteins, and a wide variety of experimental techniques have been applied to this problem. These include circular dichroism,[3] optical second-harmonic generation,[4] nuclear magnetic resonance (NMR)[5] and fluorescence spectroscopy.[6] Molecular dynamics (MD) simulations have also been used to study protein/peptide conformations.[7,8] MD simulation algorithms usually determine the trajectories of atoms and molecules by numerically solving the Newton's equations of motion for a system of interacting particles, where forces between the particles and potential energies are defined by molecular mechanics force fields. MD simulations are able to provide atomic and molecular level information needed to reveal the structures and dynamics of protein conformational change processes.

The particular problem this paper addresses is to detect conformational changes of proteins. This problem is practically important because many human diseases are associated with proteins that convert from their regular forms to abnormal ones in the affected organs. There is some evidence to suggest that diseases, such as Alzheimer's disease, Creutzfeldt-Jakob disease (mad-cow), Parkinson's disease, Huntington's disease, prion disease, and type II diabetes may be as a consequence of misfolded proteins.[9,10] The ability to detect changes in protein conformations could provide insight into the structural transition mechanisms and allow early diagnoses of diseases.

Traditional spectroscopy methods such as NMR rely on ensemble averages, that is, measurements from a large number of molecules. As a consequence, rare, but important, populations can be obscured and go undetected.[11] A technique having the ability of observing molecules one at a time is the one based on the photon counting histogram model.[12] It exploits the sensitivity of single-molecule fluorescence spec-

Received: June 22, 2014
Accepted: September 4, 2014
Published: September 4, 2014

  

troscopy to detect the presence of rare conformations of cytochrome c and thus allows more thoroughly characterizing the heterogeneity of biological samples. Single molecular fluorescence involving Förster resonance energy transfer of individual dye-labeled polyproline molecules has also been investigated.[13] Of particular note are biological and solid-state nanopores that, in addition to sequencing and detection of nucleic acids,[14] have been proposed in studying protein conformations by analyzing the characteristic transit duration times and blockade currents when a protein is translocated through the pore.[15,16]

Here we propose an alternative label-free technique that relies on the fact that conformational transitions are usually accompanied by changes in chemical and physical parameters of the proteins. In particular, as will be revealed next, each conformation carries a unique electrostatic potential (EP) signature. This opens the potential for real-time discrimination of protein conformations through examining their associated electric fields. Recent advance in nanotechnology has made it feasible to develop sensitive nanoscale sensors suitable for such applications.

## 2. RESULTS AND DISCUSSION

Our proposed device concept consists of multiple layers of graphene nanopore (GNP) sensors that measure quantum conductivity modulated by the electric fields of proteins. Graphene is a flat monolayer of carbon atoms tightly packed into a two-dimensional honeycomb lattice.[17] Because of its unique properties such as extraordinarily high electron mobility and the stability resulting from the sp2 hybridization, graphene has been regarded as a ground-breaking material for materials science and condensed-matter physics.[18] A GNP sensor is created by drilling a little hole in the interior of a graphene nanoribbon with zigzag edges (zGNR) in its width. The reason for choosing zGNRs instead of graphene nanoribbons with armchair edges is that zGNRs always remain metallic after the creation of the nanopores.[19] One distinctive feature of GNPs is that the transverse conduction currents[20,21] employed are relatively larger than the tunneling currents utilized in nanogap-based biosensors.[22] This is practically important since sufficiently large operating currents are essential for coping with interference caused by instrument and environmental noise. Single-layer GNP sensors[20,21,23−26] have been proposed as gas sensors, selective sieves for ions, and sensors for nucleobase identification.

The proposed device concept, as depicted in Figure 1, consists of multiple identical layers of GNP sensors. Because, as demonstrated by both theoretical and experimental results,[27,28] the currents of zGNRs and GNPs are mostly conducted around the edges, we introduce a horizontal vacancy gap that splits a GNP into two conduction units. With additional edges this modified GNP structure, shown in the Supporting Information, Figure S-1, has the potential of creating additional conduction channels and, therefore, enlarging operating currents. The number of layers is a design parameter and is largely determined by the size of the target protein. Enough layers are required to ensure the measurements at multiple layers collectively enable the detection of a conformational change. In the mean time, adequate interlayer spacing is required to prevent interactions between the layers. Our simulation results, shown in the Supporting Information, Figure S-2, reveal that interlayer spacing of ≥8 Å is sufficient. Since in a real biological/chemical environment the unsaturated carbon atoms

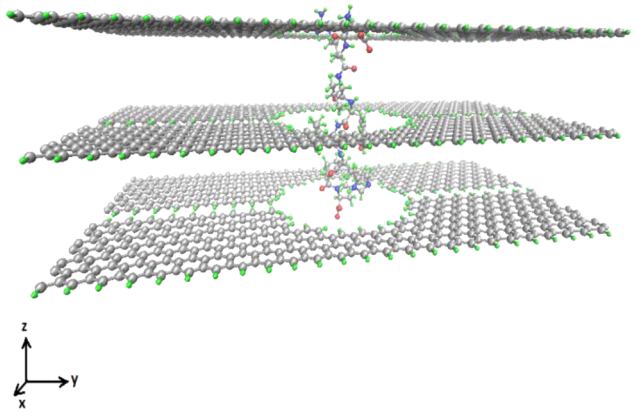


**Figure 1.** Schematic view of the proposed device concept consisting of multiple identical layers of GNP sensors. The number of GNP layers is chosen to be 3 with interlayer spacing 10 Å. The geometries of the GNP sensors can be found in the Supporting Information, Figure S-1. The GNP sensors are positioned in the xy planes with the middle layer located at $z = 0$. Also shown is an Angiotensin II molecule placed inside the device with geometrical center coinciding with that of the middle layer. The left and right sides of each GNP are to be connected to electrodes and currents flow horizontally in the $y$ direction across the device.

on ribbon- and pore-edges would tend to capture ions to satisfy their dangling bonds, in our study they are passivated with hydrogen atoms.[29] Note that other forms such as nitrogen-passivated[30,31] or self-reconstructed[32] GNPs can also be used.

As compared with biological and solid-state nanopores that measure ensemble properties such as translocation duration and blockade current,[15,16] this proposed device concept allows more detailed examination of the molecules being tested with high spatial resolution, utilizing the one-atom-thickness feature of GNP sensors. The sensing principle is that the characteristic EP generated by protein molecules changes the electron charge distribution around each of the pores and, thereby, modulates the currents flowing across the GNP sensors. Since the EP is closely associated with the geometries of the protein constituent atoms, the current modulations at multiple locations measured by the GNP sensors collectively serve as a metric for protein conformational discrimination.

In our study, we use conformations of Angiotensin II obtained through MD simulations, shown in Figure 2. Angiotensin II is an octapeptide hormone derived from the precursor molecule angiotensinogen, a serum globulin produced constitutively and released into the circulation mainly by the liver. It plays a central role in cardiovascular homeostasis by acting as a vasoactive agonist and inducing contraction of blood vessels. Angiotensin II has been shown to play important roles in mediating hypertension, heart failure, cardiac remodeling, diabetes, and the proliferative and inflammatory responses to arterial injury.[33]

Our MD simulation process is as follows. First, amino acids residuals of Angiotensin II, namely, Asp-Arg-Val-Tyr-Ile-His-Pro-Phe, are input to the molecular building and visualizing computer tool VMD[34] to obtain initial conformers with arbitrary folding states. An initial conformer is then solvated in a 40 Å × 40 Å × 40 Å water box, creating a system of ∼5800 atoms. Finally, each system assembled with different initial Angiotensin II conformers undergoes 5000-step energy minimization followed by 5 ns equilibration to obtain low energy configuration states. Since a protein molecule possesses

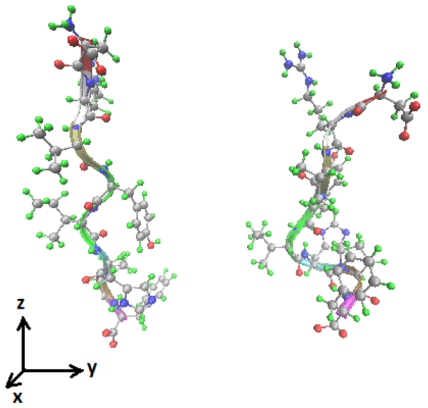


**Figure 2.** Conformations of Angiotensin II obtained through MD simulations. The carbon, hydrogen, oxygen and nitrogen atoms are colored silver, green, red and blue, respectively. The backbones are further displayed in ribbon representations. The left and right conformations will be referred to as C1 and C2, respectively.

a molecular dipole moment resulting from nonuniform distributions of positive and negative charges on constituent atoms, during the energy minimization and equilibration process a mild electrical field of 0.2 kcal/(mol Å e) across the system in the $-z$ direction is applied to orientate the protein conformations along the $z$ axis. The final geometries of Angiotensin II reached by the simulated systems are used as our test conformations. The MD simulation package NAMD[35] with CHARMM27[36] force field is utilized in the simulations, where the system temperature is set to be 300 K, time step 1 fs and geometries sampled every picosecond. Two acquired conformations of Angiotensin II are shown in Figure 2. Note that we are not intending to conduct a comprehensive study of folding/unfolding processes of Angiotensin II. The purpose here is to obtain different conformations and, in our subsequent study, show marked differences in their EP profiles and demonstrate the feasibility of discriminating between them with our proposed device concept.

The two conformations shown in Figure 2 are similar in shape and size, measuring ∼1.3 nm in diameter and ∼2.5 nm in length along the $z$ direction. Figure 3 shows the electrostatic difference potential ($\Delta V_H$) of Angiotensin II in these conformations, evaluated at cross sections $z$ = 10 Å, 0 and −10 Å, where $z$ = 0 corresponds to the geometrical center of the conformations. The quantity $\Delta V_H$ describes the electrostatic potential landscape that causes changes in the electron charge distribution compared to the neutral system, i.e., the case when the atoms are just put together but no interactions between them is turned on,[37] and thus describes the induced electric field. For this computation and subsequent GNP quantum transport study, we employ the density functional based tight binding (DFTB) method.[38,39] The DFTB formalism is an approximate method based on a second-order expansion of the Kohn−Sham total energy in density-functional theory (DFT) with respect to charge density fluctuations. It expresses the transmission in terms of nonequilibrium Greens function and computes conductance using the Landauer formula. In DFTB only small numbers of empirical parameters are used and they are consistently obtained from DFT calculations. It has been shown that DFTB, especially its self-consistent charge extension (SCC-DFTB) holds nearly the same accuracy as DFT, but at much lower computational costs, allowing investigation of the electronic structure of large

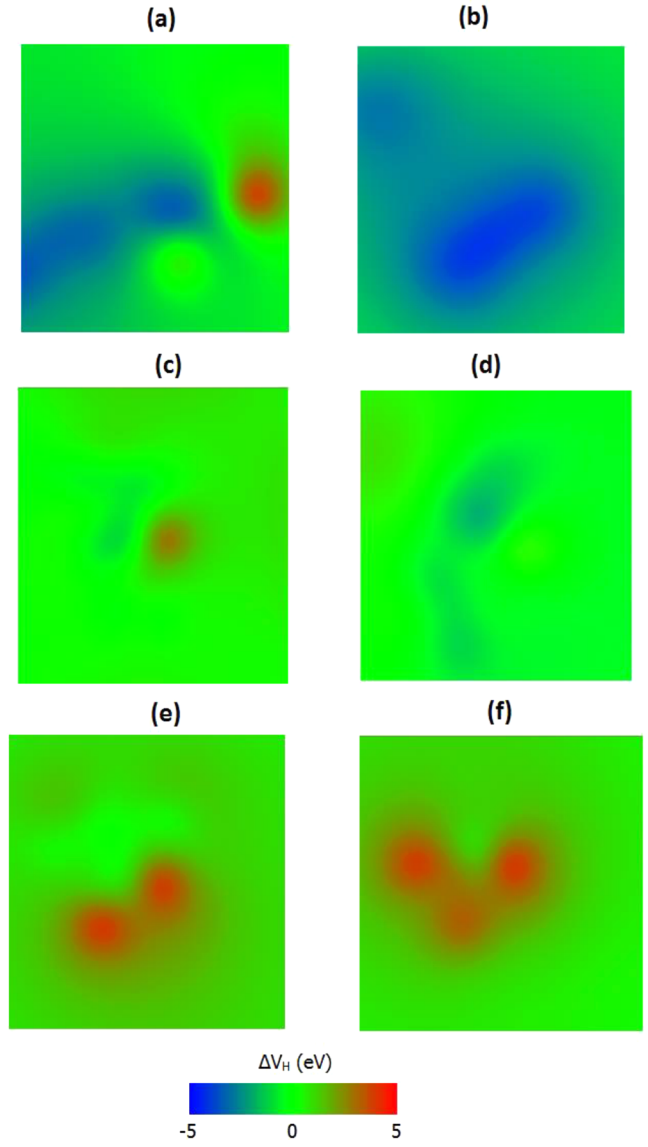


**Figure 3.** Electrostatic difference potential of Angiotensin II in the two conformations (C1 and C2) shown in Figure 2. Examined at different cross sections along the $z$ direction, with $z$ = 0 corresponding to the geometrical center. (a) C1 at $z$ = 10 Å; (b) C2 at $z$ = 10 Å; (c) C1 at $z$ = 0; (d) C2 at $z$ = 0; (e) C1 at $z$ = −10 Å; (f) C2 at $z$ = −10 Å.

systems.[40] DFTB schemes have been successfully used in a wide range of applications, from molecular compounds, to systems in solid state. The SCC-DFTB implementation of the commercial package Atomistix ToolKit (ATK) from QuantumWise[41] is utilized in our study.

As can be seen in Figure 3, the EP critically depends on the geometries of the constituent atoms. This is understandable since EP is the result of interactions among electric charges of these atoms. Both conformations show lower EP values toward the top end (i.e., around $z$ = 10 Å) and higher EP values toward the bottom end (i.e., around $z$ = −10 Å), due to the positively charged N- and C- terminals located near the two ends, respectively. The Supporting Information, Figure S-3, depicts the isosurfaces of these EP profiles. There, it can be seen that it is possible for different conformations to exhibit similar EP at a particular location. However, even for conformations with small difference in shape and size as shown in Figure 2, the EP

profiles examined at multiple cross-sections collectively constitute a signature unique to each conformation, as demonstrated in Figure 3.

We now evaluate how Angiotensin II molecules in different conformations modulate conductivity with our proposed device concept, where each of the GNP layer is constructed by first drilling a pore of diameter 1.8 nm in the center of a zGNR with 14 zigzag chains (~2.8 nm in width), and then splitting in the middle with a 2.5 Å vacancy gap. The geometries of the GNP after passivation and energy minimization can be found in the Supporting Information, Figure S-1. The number of GNP layers is chosen to be 3 with interlayer spacing 10 Å. The GNP sensors are positioned in the *xy* planes with the middle layer located at $z = 0$. The Angiotensin II molecule is placed inside the device with geometrical center coinciding with that of the middle layer, as shown in Figure 1. Prior to conductivity calculation, the geometries of the system are optimized by relaxing the atom coordinates so that the forces on individual atoms are minimized to be smaller than 0.05 eV/Å. The self-consistent DFTB basis set CP2K as implemented in the ATK package[41] is used and simulation parameters are set as follows: temperature 300 K, energy mesh cutoff 10 hartree, max interaction range 10 Å and k-point sampling (1, 1, 100). The Angiotensin II modulated zero-bias quantum conductance (in units of $G_0 = 2e^2/h = 7.75 \times 10^{-5}\ \Omega^{-1}$) of the GNP sensors are shown in Figure 4, where each conductance is the average over four orientations (rotating along the *z* axis by 0°, 90°, 180°, and 270°, respectively) of each Angiotensin II conformation.

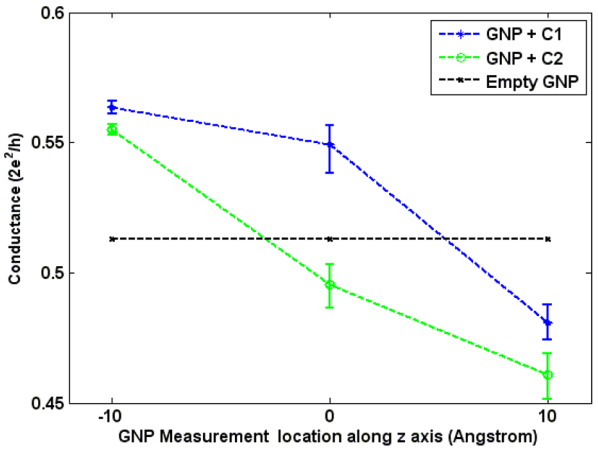


**Figure 4.** Zero-bias conductance of GNP sensors modulated by Angiotensin II in the two conformations (C1 and C2) shown in Figure 2. Unit of conductance is $G_0 = 2e^2/h$ with $e$ denoting the electronic charge and $h$ Planck constant. Also shown is the GNP conductance without the presence of Angiotensin II.

As shown in Figure 4, the conductance of each empty GNP sensor (i.e., without the presence of Angiotensin II) is $0.513G_0$. Referring to the EP of Angiotensin II examined at various cross sections shown in Figure 3, one can see that the positively charged N-terminal (lower EP values) reduces the conductivity, whereas the negatively charged C-terminal (higher EP values) enhances the GNP conductivity. This is supported by the Supporting Information, Figure S-4, where the difference between the electrostatic difference potential at the GNP located near the N-terminal (i.e., at $z = 10$ Å) and that at the GNP located near the C-terminals (i.e., at $z = -10$ Å) is obvious. In other words, the introduction of Angiotensin II can either boost or hinder the original electric current in the GNP sensors, depending on how the electron charge densities around the measurement locations are modulated. More importantly, Figure 4 reveals that the measured GNP conductance spectra, that is, the conductance obtained at multiple locations, are distinctive for different conformations. Most notably, the middle layer GNP sensor has conductance $0.549G_0$ and $0.495G_0$ for conformations C1 and C2, respectively, leading to a conductance difference of $0.054G_0$. This can be understood by comparing the difference between the C1-induced electrostatic difference potential $\Delta V_{H\_C1}$(shown in the Supporting Information, Figure S-5a) and C2-induced electrostatic difference potential $\Delta V_{H\_C2}$ (shown in the Supporting Information, Figure S-5b), as depicted in the Supporting Information, Figure S-6. This conformation-induced conductance difference corresponds to ~0.42 $\mu$A current difference under a moderate bias voltage of 0.1 V. This significant difference in current would be readily detectable even under strong interference caused by thermal vibrations and instrument noise.

## 3. CONCLUSION

We have proposed a new device concept consisting of multiple layers of GNP sensors for the detection of protein conformational changes. Each layer measures the effect of protein-produced electric field on quantum conductance at a certain location. Because of the distinctiveness of EP profiles associated with each protein conformation, the currents flowing across the GNP sensors constitute a signature characteristic to each conformation, enabling reliable discrimination between protein conformations.

## ■ ASSOCIATED CONTENT

### Ⓢ Supporting Information

Figure S-1: Geometry of the optimized hydrogen-passivated GNP sensor. Figure S-2: Geometry of optimized multilayer GNPs with 8 Å interlayer spacing. Figure S-3: Isosurfaces of electrostatic difference potential of Angiotensin II in different conformations. Figure S-4: Electrostatic difference potential measured at the GNP sensors. Figure S-5: Electrostatic difference potential measured at the GNP sensor located at $z = 0$ when Angiotensin II with different conformations is present. Figure S-6: Difference between the conformation-induced electrostatic difference potential measured at the GNP located at $z = 0$. This material is available free of charge via the Internet at http://pubs.acs.org.

## ■ AUTHOR INFORMATION

### Corresponding Author

*E-mail: sskaf@unimelb.edu.au.

### Notes

The authors declare no competing financial interest.

## ■ REFERENCES

(1) Simmerling, C.; Strockbine, B.; Roitberg, A. E. All-Atom Structure Prediction and Folding Simulations of a Stable Protein. *J. Am. Chem. Soc.* **2002**, *124*, 11258−11259.

(2) Valdes, H.; Pluháčková, K.; Pitonák, M.; Řezáč, J.; Hobza, P. Benchmark Database on Isolated Small Peptides Containing an Aromatic Side Chain: Comparison between Wave Function and Density Functional Theory Methods and Empirical Force Field. *Phys. Chem. Chem. Phys.* **2008**, *10*, 2747−2757.

(3) Streicher, W. W.; Makhatadze, G. I. Unfolding Thermodynamics of Trp-Cage, a 20 Residue Miniprotein, Studied by Differential Scanning Calorimetry and Circular Dichroism Spectroscopy. *Biochemistry* **2007**, *46*, 2876−2880.
(4) Salafsky, J. S. Detection of Protein Conformational Change by Optical Second-Harmonic Generation. *J. Chem. Phys.* **2006**, *125*, 074701.
(5) Neidigh, J. W.; Fesinmeyer, R. M.; Andersen, N. H. Designing a 20-Residue protein. *Nat. Struct. Biol.* **2002**, *9*, 425−430.
(6) Calleja, V.; Ameer-Beg, S.; Vojnovic, B.; Woscholski, R.; Downward, J.; Larijani, B. Monitoring Conformational Changes of Proteins in Cells by Fluorescence Lifetime Imaging Microscopy. *Biochem. J.* **2003**, *372*, 33−40.
(7) Wu, X.; Yang, G.; Zu, Y.; Fu, Y.; Zhou, L.; Yuan, X. Molecular Dynamics Characterisations of the Trp-Cage Folding Mechanisms: In the Absence and Presence of Water Solvents. *Mol. Simul.* **2012**, *38*, 161−171.
(8) Colombo, G.; Roccatano, D.; Mark, A. E. Folding and Stability of the Three-Stranded $\beta$ Sheet Peptide Betanova: Insights from Molecular Dynamics Simulations. *Proteins: Struct., Funct., Genet.* **2002**, *46*, 380−392.
(9) Chiti, F.; Dobson, C. M. Protein Misfolding, Functional Amyloid, and Human Disease. *Annu. Rev. Biochem.* **2006**, *75*, 333−366.
(10) Wu, K. P.; Weinstock, D. S.; Narayanan, C.; Levy, R. M.; Baum, J. Structural Reorganization of $\alpha$-Synuclein at Low pH Observed by NMR and REMD Simulations. *J. Mol. Biol.* **2009**, *391*, 784−796.
(11) Perroud, T. D.; Bokoch, M. P.; Zare, R. N. Cytochrome c Conformations Resolved by the Photon Counting Histogram: Watching the Alkaline Transition with Single-Molecule Sensitivity. *Proc. Natl. Acad. Sci. U.S.A.* **2005**, *102*, 17570−17575.
(12) Lindhoud, S.; Westphal, A. H.; Visser, A. J.; Borst, J. W.; van Mierlo, C. P. Fluorescence of Alexa Fluor Dye Tracks Protein Folding. *PLoS One* **2012**, *7*, e46838.
(13) Perroud, T. D.; Huang, B.; Zare, R. N. Effect of Bin Time on the Photon Counting Histogram for One-Photon Excitation. *ChemPhysChem* **2005**, *6*, 905−912.
(14) Ying, Y.-L.; Zhang, J.; Gao, R.; Long, Y.-T. Nanopore-Based Sequencing and Detection of Nucleic Acids. *Angew. Chem., Int. Ed.* **2013**, *52*, 13154−13161.
(15) Shasha, C.; Henley, R. Y.; Stoloff, D. H.; Rynearson, K. D.; Hermann, T.; Wanunu, M. Nanopore-Based Conformational Analysis of a Viral RNA Drug Target. *ACS Nano* **2014**, *8*, 6425−6430.
(16) Wang, H.-Y.; Ying, Y.-L.; Li, Y.; Kraatz, H.-B.; Long, Y.-T. Nanopore Analysis of $\beta$-Amyloid Peptide Aggregation Transition Induced by Small Molecules. *Anal. Chem.* **2011**, *83*, 1746−1752.
(17) Geim, A. K.; Novoselov, K. S. The Rise of Graphene. *Nat. Mater.* **2007**, *6*, 183−191.
(18) Li, H.; Xu, C.; Srivastava, N.; Banerjee, K. Carbon Nanomaterials for Next-Generation Interconnects and Passives: Physics, Status, and Prospects. *IEEE Trans. Electron Devices* **2009**, *56*, 1799−1821.
(19) Qiu, W.; Nguyen, P.; Skafidas, E. Graphene Nanopores: Electronic Transport Properties and Design Methodology. *Phys. Chem. Chem. Phys.* **2014**, *16*, 1451−1459.
(20) Nelson, T.; Zhang, B.; Prezhdo, O. V. Detection of Nucleic Acids with Graphene Nanopores: Ab Initio Characterization of a Novel Sequencing Device. *Nano Lett.* **2010**, *10*, 3237.
(21) Saha, K. K.; Drndić, M.; Nikolić, B. K. DNA Base-Specific Modulation of Microampere Transverse Edge Currents Through a Metallic Graphene Nanoribbon with a Nanopore. *Nano Lett.* **2012**, *12*, 50−55.
(22) Prasongkit, J.; Grigoriev, A.; Pathak, B.; Ahuja, R.; Scheicher, R. H. Transverse Conductance of DNA Nucleotides in a Graphene Nanogap from First Principles. *Nano Lett.* **2011**, *11*, 1941−1945.
(23) Jiang, D.; Cooper, V. R.; Dai, S. Porous Graphene as the Ultimate Membrane for Gas Separation. *Nano Lett.* **2009**, *9*, 4019.
(24) Blankenburg, S.; Bieri, M.; Fasel, R.; Mullen, K.; Pignedoli, C. A.; Passerone, D. Porous Graphene as an Atmospheric Nanofilter. *Small* **2010**, *6*, 2266.
(25) Sint, H.; Wang, B.; Král, P. Selective Ion Passage through Functionalized Graphene Nanopores. *J. Am. Chem. Soc.* **2008**, *130*, 16448.
(26) Qiu, W.; Skafidas, E. Gapped Graphene Nanopores with Enhanced Operating Current and Sensitivity for Biological and Chemical Sensing applications. *Appl. Phys. Lett.* **2014**, *105*, 033104.
(27) Jia, X.; Hofmann, M.; Meunier, V.; et al. Controlled Formation of Sharp Zigzag and Armchair Edges in Graphitic Nanoribbons. *Science* **2009**, *323*, 1701−1705.
(28) Chang, P. H.; Nikolić, B. K. Edge Currents and Nanopore Arrays in Zigzag and Chiral Graphene Nanoribbons as a Route toward High-ZT Thermoelectrics. *Phys. Rev. B* **2012**, *86*, 041406(R).
(29) Cai, J.; Ruffieux1, P.; Jaafar, R.; et al. Atomically Precise Bottom-up Fabrication of Graphene Nanoribbons. *Nature* **2010**, *466*, 470−473.
(30) Wang, X.; Li, X.; Zhang, L.; Yoon, Y.; Weber, P. K.; Wang, H.; Guo, J.; Dai, H. N-Doping of Graphene through Electrothermal Reactions with Ammonia. *Science* **2009**, *324*, 768−771.
(31) Al-Dirini, F.; Hossain, F. M.; Nirmalathas, A.; Skafidas, E. All-Graphene Planar Self-Switching MISFEDs, Metal-Insulator-Semiconductor Field-Effect Diodes. *Sci. Rep.* **2014**, *4*, 3983.
(32) Song, L. L.; Zheng, X. H.; Wang, R. L.; Zeng, Z. Dangling Bond States, Edge Magnetism, and Edge Reconstruction in Pristine and B/N-Terminated Zigzag Graphene Nanoribbons. *J. Phys. Chem. C* **2010**, *114*, 12145−12150.
(33) Taubman, M. B. Angiotensin II: A Vasoactive Hormone with Ever-Increasing Biological Roles. *Circ. Res.* **2003**, *92*, 9−11.
(34) Humphrey, W.; Dalke, A.; Schulten, K. VMD: Visual Molecular Dynamics. *J. Mol. Graphics* **1996**, *14*, 33−38.
(35) Phillips, J. C.; Braun, R.; Wang, W.; Gumbart, J.; Tajkhorshid, E.; Villa, E.; Chipot, C.; Skeel, R. D.; Kalé, L.; Schulten, K. Scalable Molecular Dynamics with NAMD. *J. Comput. Chem.* **2005**, *26*, 1781−1802.
(36) Foloppe, N.; MacKerell, A. D. All-Atom Empirical Force Field for Nucleic Acids: I. Parameter Optimization Based on Small Molecule and Condensed Phase Macromolecular Target Data. *J. Comput. Chem.* **2000**, *21*, 86−104.
(37) Soler, J. M.; Artacho, E.; Gale, J. D.; Garcia, A.; Junquera, J.; Ordejon, P.; Sanchez-Portal, D. The SIESTA Method for Ab Initio Order-N Materials Simulation. *J. Phys.: Condens. Matter* **2002**, *14*, 2745.
(38) Elstner, M.; Porezag, D.; Jungnickel, G.; Elsner, J.; Haugk, M.; Frauenheim, Th.; Suhai, S.; Seifert, G. Self-Consistent-Charge Density-Functional Tight-binding Method for Simulations of Complex Materials Properties. *Phys. Rev. B* **1998**, *58*, 07260.
(39) Brandbyge, M.; Mozos, J.-L.; Ordejón, P.; Taylor, J.; Stokbro, K. Density-Functional Method for Nonequilibrium Electron Transport. *Phys. Rev. B* **2002**, *65*, 165401.
(40) Oliveira, A. F.; Seifert, G.; Heine, T.; Duarte, H. A. Density-Functional Based Tight-Binding: An Approximate DFT Method. *J. Braz. Chem. Soc.* **2009**, *20*, 1193−1205.
(41) Atomistix ToolKit version 12.8.2, QuantumWise A/S (www.quantumwise.com).